Image Plate Multi-Scan Response to Fusion Protons in the range of 1 - 14 MeV

N. Vanderloo,[1] M. Cufari,[1] L. Russell,[1] T.M. Johnson,[1] J. Vargas,[1] B.C. Foo,[1] B.I. Buschmann,[1] S.G. Dannhoff,[1] A. DeVault,[1] T.E. Evans,[1] J.H. Kunimune,[1] Y. Lawrence,[1] J.A. Pearcy,[1] B.L. Reichelt,[1] C.W. Wink,[1] M. Gatu Johnson,[1] R.D. Petrasso,[1] J. A. Frenje,[1] and C. K. Li[1]
Plasma Science and Fusion Center: MIT. Cambridge, MA 02139

(*Electronic mail: nielsv@mit.edu)

(Dated: 12 July 2024)

Image plates (IPs) are a quickly recoverable, and reusable radiation detector often used to measure proton and x-ray fluence in laser-driven experiments. Recently, IPs have been used in a proton radiography detector stack on the OMEGA laser, a diagnostic historically implemented with CR-39 or radiochromic film. The IPs used in this, and other diagnostics detect charged particles, neutrons, and x-rays indiscriminately. IPs detect radiation using a photo-stimulated luminescence (PSL) material, often phosphor, in which electrons are excited to metastable states by ionizing radiation. Protons at MeV energies deposit energy deeper into the IP compared with x-rays below ∼20 keV due to the Bragg peak present for protons. This property is exploited to discriminate between radiation type. Doses of mono-energetic protons between 1.7 MeV and 14 MeV are applied to IPs using the MIT Linear Electrostatic Ion Accelerator. This paper presents the results from consecutive scans of IPs irradiated with different proton energies. The PSL ratios between subsequent scans are shown to depend on proton energy, with higher energy protons having lower PSL ratios for each scan. This finding is separate from the known energy dependence in absolute sensitivity of IPs. The results can be compared to complimentary work on x-rays, showing a difference between protons and x-rays, forging a path to discriminate between proton and x-ray fluence in mixed radiation environments.

I. INTRODUCTION

In laser-driven plasma experiments, measurements of ionizing radiation provide key insights into the dynamics and conditions of the plasma under study. Many radiation detectors exist, including scintillators, radiochromic film (RCF), nuclear track detectors such as CR-39, and imaging plates (IPs). On large laser platforms including OMEGA, LULI 2000, and the NIF, diagnostic tools often employ IPs to measure the spatial distribution of highly energetic photons, and charged particles[1,2,3,4,5]. IPs offer distinct advantages in their versatility; they detect charged particles, photons and neutrals, they are reusable, and their data can be quickly recovered.

For proton detection, IPs may be compared with a popular solid state nuclear track detector like CR-39. Data turnaround for IPs is on the order of tens of minutes, whereas the chemical etching process for CR-39 data requires a few hours at the least, often stretching the entire recovery process to days or weeks. This advantage of IPs becomes extremely useful for time sensitive experiments like those on OMEGA or the NIF, where laser access is highly competitive and limited to a small number of shots sometimes just hours apart. One significant pitfall of IPs for proton detection is that they also indiscriminately detect photons. Understanding the differences in how an IP responds to charged particles and photons is crucial.

Proton radiography is a common diagnostic for laser-driven plasma experiments that relies on an accurate measurement of the spatial distribution of protons[6]. The diagnostic probes at the electric and magnetic fields present in a plasma by characterizing how a stream of protons is deflected within the plasma by the Lorentz $\mathbf{E} + (\mathbf{v} \times \mathbf{B})$ force. The proton stream is either produced by using target normal sheath acceleration (TNSA)[7], which provides a broad energy spectrum, or D-^{3}He gas-filled so called "exploding pushers", shock driven implosions that produce mono-energetic 3.0 MeV and 14.7 MeV protons from D-D and D-^{3}He fusion reactions, respectively[8]. Historically, proton radiography has used CR-39 (exploding pushers)[9,10] or RCF (TNSA)[7] to measure the flux of deflected protons, until recently when E.R. Tubman et al. [2] used IPs in a proton-radiography stack in an exploding pusher experiment.

The absolute sensitivity of IPs to protons has been studied[11,12,13], but one unresolved issue with IP proton-radiography is that the exploding pushers also produce electrons, neutrons, and x-rays that affect the proton data. In particular, IPs are highly sensitive to x-rays. In the E.R. Tubman et al. [2] experiment, a 250μm Ta filter was used to block the soft x-rays produced by the exploding pusher. Another IP was placed behind the first to subtract the hard x-rays (those that penetrate both the filter and first IP) in post-processing. However, there are intermediate energy x-rays that are neither blocked nor subtracted. Additionally, the Ta filter removes all signal from the 3 MeV fusion protons. It is especially problematic to remove the 3 MeV protons because lower energy protons are deflected more by the **E** and **B** fields and provide more insight when weaker fields are present.

In this paper, we exploit the ability of IPs to be scanned multiple times and find that there is a derived quantity, the ratio between scan intensities, that depends on proton energy. A complimentary paper by M. Cufari et al. [14] shows that the same is also true for IPs irradiated with x-rays. These two findings, in conjunction, lay the groundwork for resolving the issue of IPs irradiated with a mixed proton-x-ray fluence, an issue, which occurs in proton radiography and x-ray diagnostics.

II. IMAGING PLATES

IPs are a type of radiation detector initially developed for use in medical applications, but later adapted for use in laser-driven plasma physics experiments. The active layer of an IP is a phosphor film that excites electrons to metastable F-centers when exposed to ionizing radiation. The trapped elec-

TABLE I. Material compositions of IP layers given by the manufacturer.

Layer	MS	SR
Protective	C_2H_2O	C_2H_2O
Thickness (μm)	9	6
Density (g/cm^3)	1.66	1.273
Phosphor	$BaFBr_{0.85}I_{0.15}$	BaFBr
Thickness (μm)	115	120
Density (g/cm^3)	3.31	3.1
Supportive	C_2H_2O	C_2H_2O
Thickness (μm)	190	188
Density (g/cm^3)	1.66	1.273
Magnetic	$ZnMn_2Fe_5NO_{40}H_{15}C_{10}$	(same as MS)
Thickness (μm)	160	160
Density (g/cm^3)	2.77	3.1

trons can be brought back to the ground state by incident visible light, emitting light with intensity proportional to the number of trapped electrons. A visible light red laser is used to knock electrons out of the F-centers in a pinpoint region of the IP; scanning the laser across the IP and recording the light emission with a photomultiplier tube (PMT) constructs a digital image of the IP. This emission is called photo-stimulated luminescence (PSL). The remaining signal on the IP can be subsequently erased by broad spectrum visible light for reuse. Unintentional erasure can occur if the IP is exposed to bright lights in the laboratory. The IPs in this experiment were handled in the dark.

The IPs are also subject to a nonlinear fading due to thermal effects; the PSL decays as a function of time between irradiation and scanning. This decay curve has been quantified and is often expressed as a sum of multiple exponential functions with different decay constants[15]. The specifics of the decay constants and corresponding profile depend on factors such as IP type, radiation type, scanner type, and temperature. The fading has been characterized for the IPs used in this experiment[13,16], but a specific numerical fade correction was not needed here as the fade time was held constant throughout. The time interval between exposure and scans were the same for each piece (30 min). It is worth noting that, when scanning multiple times, fading affects the first scan most strongly, and the subsequent scans substantially less so[17].

Two IP variants are considered in this experiment: the Fujifilm BAS-SR, and BAS-MS types. The SR (Super Resolution) type includes a blue pigment designed to decrease scattering of the scanning laser, thereby increasing the resolution of the scan. The MS (Multipurpose Standard) type does not contain a dye and is the most sensitive to ionizing radiation, meaning the PSL per dose is highest[16]. The IPs consist of four layers, a thin protective film, the active phosphor layer, a thick supportive layer, and a magnetic layer used to attach the IP to the scanning system. The various material properties of these IPs are given by the manufacturer and listed in Table I.

III. METHOD

There are two experimental procedures that are important to consider in this experiment: the irradiation of IPs with protons, and the scanning of IPs to obtain data.

To irradiate IPs with protons at energies relevant to proton

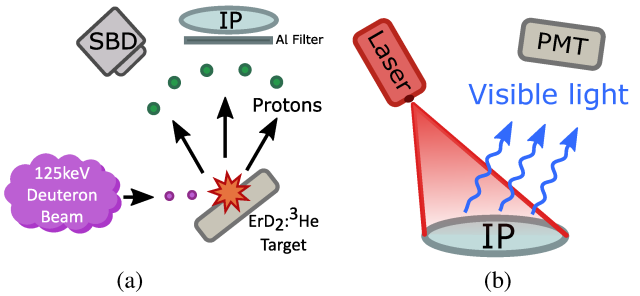

FIG. 1. (a) The experimental setup for irradiating IPs with monoenergetic protons. A 125 keV deuteron beam was incident on a helium-3 doped erbium-deuteride target causing D-D and D-^{3}He fusion reactions. An SBD placed 35° off of the target-IP axis was used to evaluate accelerator performance by counting incident protons. (b) A schematic for the scans performed using an Cytiva Amersham™ Typhoon™ scanner. A 635 nm laser scans the IP and a PMT was used to measure the PSL.

radiography, fusion reactions were generated using a beam-target fusion setup on the Linear Electrostatic Ion Accelerator at MIT[18]. The experiment is depicted schematically in Figure 1(a). Deuterons are accelerated by a 125 kV potential with the beam incident on a helium-3 doped 30μm thick erbium-deuteride target. Helium-3 target doping is performed in a separate procedure where the beam species is replaced with 80keV helium-3 ions[18]. The deuterium beam-target reactions produce protons that emit radially from the target. The exact energies of the protons produced depends on the angle they emit from the target. At 90° from the deuteron beam axis, the fusion reactions and particle energies are given by[19]

$$\mathrm{D}+\mathrm{D}\rightarrow \mathrm{T}\,(1.01\,\mathrm{MeV})+\mathrm{p}\,(3.02\,\mathrm{MeV}) \quad (\sim 50\%), \tag{1}$$
$$\mathrm{D}+\mathrm{D}\rightarrow {}^3\mathrm{He}(0.82\,\mathrm{MeV})+\mathrm{n}\,(2.45\,\mathrm{MeV}) \quad (\sim 50\%), \tag{2}$$
$$\mathrm{D}+{}^3\mathrm{He}\rightarrow \alpha\,(3.7\,\mathrm{MeV})+\mathrm{p}\,(14.7\,\mathrm{MeV}). \tag{3}$$

In this experiment, tritons, helium-3 ions, and alphas were ranged out by all considered filtering configurations, and IP sensitivity to neutrons is low[20]. Hence, signal on the IP is dominated by protons. An IP cut to a 5 cm diameter circle is placed 10 cm from the target center and offset 90° from the beam axis. An ORTEC® silicon surface barrier detector (SBD) is placed at the same height as the IP, 17 cm from the target center, and offset 125° from the beam line. A 15μm Ta filter is placed in front of the SBD to block beam deuterons. The SBD measures the energies of incident protons over the course of the experiment. The number of protons counts per second is used to assess accelerator performance. However, fusion protons produced at different laboratory angles have different energies. As the protons incident on the SBD were produced at a different angle than those on the IP, the off-axis SBD spectrum does not reveal information about the protons incident on the IP. The chamber containing the target, SBD, and IP is held at high vacuum.

Due to the nature of the fusion reactions listed above, the energy spectrum of protons incident on the IP should be centered around 3.02 MeV and 14.7 MeV. However, there is broadening in the energy due to fusion reactions occurring at different depths in the target, and the 28° difference in laboratory angle between the left and right sides of the IP. A beam-target physics simulation[18] was performed to estimate the total energy broadening of the D-D protons incident on

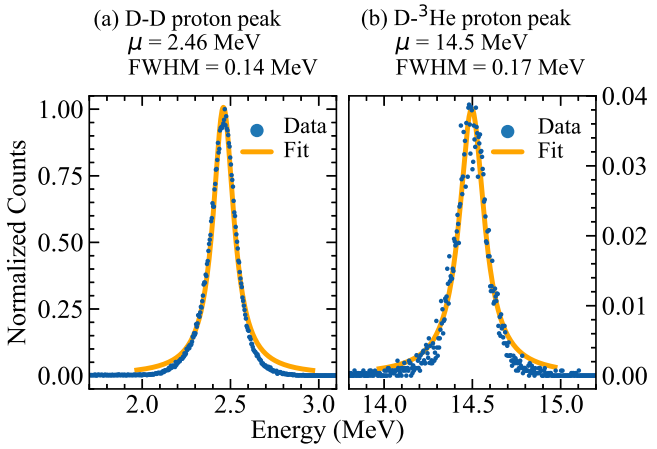

FIG. 2. (a) The energy spectrum of D-D protons measured with an SBD positioned at an angle of 90° relative to the incoming beam. The SBD had 25μm of Al positioned in front. (b) The energy spectrum of D-^{3}He protons incident on the same SBD with the same filter. Both spectra are normalized to the D-D peak height of ~700,000 counts/MeV. Each spectrum is modeled by a Lorentzian function with central energy μ and FWHM listed.

the IP. The D-^{3}He reactions were not simulated. The mean energy of D-D protons incident on the IP (before filtering) was simulated to be 3.0 MeV with a 0.2 MeV full width at half maximum (FWHM).

To measure the spectrum of protons where the IP is positioned, a separate experiment (with no IP) was performed with the SBD positioned 10 cm from the target at an angle of 90° relative to the direction of the incoming beam. A 25μm Al filter was placed in front of the SBD. The SBD was irradiated for thirty minutes; the resulting spectra are shown in Figure 2 with the spectrometer counts normalized to the D-D peak height. The D-D and D-^{3}He spectra were modeled with a Lorentzian function. The central energy of the D-D proton spectrum after filtering was determined to be 2.46 MeV with 0.14 MeV FWHM and the D-^{3}He spectrum was fit to be 14.50 MeV with 0.17 MeV FWHM. The spectrum is expected to be slightly wider for protons incident on the IP as the SBD aperture (0.172 cm^2) is smaller than the IP size. Hence, there is more angular spread in protons incident on the IP. This was taken into account in the kinematic simulation. The simulation results, 3.0 MeV ranged down by filtering to 2.4 MeV, are in agreement with the measured D-D spectrum. The 14.7 MeV D-^{3}He protons are expected, from SRIM stopping power tables[21], to be ranged down to 14.5 MeV, in agreement with the measured D-^{3}He spectrum.

Both SR and MS type IPs were irradiated in six separate experiments performed on different days. For both IP variants, three different filters were placed on top of the IP's protective layer, entirely covering it. The aluminum filters were were nominally 25, 50 and 100μm thick. Based on SRIM stopping power tables[21], the 100μm filter entirely blocks the D-D proton signal, isolating the D-^{3}He proton signal, ranging it down from the birth 14.7 MeV to 14.0 MeV. The 25 and 50μm filters attenuate the D-D protons from 3.0 MeV to 2.4 MeV and 1.7 MeV, respectively. The D-^{3}He protons penetrate too and are attenuated from 14.7 MeV to 14.5 MeV and 14.4 MeV, respectively. The SBD spectrum shown in Figure 2 confirms the results computed with SRIM. However, less than 5% of the total reactions were D-^{3}He, and the IP is less than 20% as sensitive to ~14.5 MeV protons than ~2 MeV protons[11], so the D-^{3}He protons make up less than 1% of the total IP signal.

TABLE II. For each experimental combination of IP type and proton energy: the mean scanner saturation for the first scan, the computed PSL, and the relative standard deviation of the corresponding distribution are given. The scanner saturation is linearly proportional to the IP PSL level.

IP type	E (MeV)	Scanner saturation on Scan 1 (0-1)	PSL per pixel	Relative σ
MS	1.7	0.034	2.4	25%
MS	2.4	0.19	15	18%
MS	14.0	0.04	3.2	15%
SR	1.7	0.037	2.9	16%
SR	2.4	0.042	3.3	12%
SR	14.0	0.004	0.3	27%

In each case, the IPs were exposed to radiation for thirty minutes. The exposure time was held constant to keep PSL fading effects consistent between cases. This is important because fading occurs not only between exposure and scanning, but also during the course of exposure. However, due to the smaller number of D-^{3}He reactions compared with D-D, and fluctuations in accelerator performance, the dose between different thirty minute exposures is *not* expected to be similar. In M. Cufari et al.[14] it was shown that the dose does not affect the PSL ratio between scans for IPs irradiated with x-rays. While a similar outcome is expected with protons, it is not known for certain what the effect of dose variation is on the PSL ratio between scans.

After exposing the IPs to radiation they were transferred in a dark room to a Cytiva Amersham™ Typhoon™ for scanning exactly thirty minutes after irradiation. The 635 nm scanning laser sweeps over the IP for approximately 5 minutes with a 50 μm pixel size. Note that while the pixel size is 50 μm, this is set by the sampling interval, the laser spot size is expected to be larger. Five total scans are completed in succession without moving the IP. The PSL for each pixel is measured by a PMT and stored as a compressed 16 bit value. The compressed value, $C \in [0, 2^{16}-1]$, is converted to the fraction of PMT saturation, $S \in [0,1]$ using the formula

$$S = 10^{5\left(\frac{C}{2^{16}-1}-1\right)} \tag{4}$$

given by Cytiva. The percentage S is referred to as the "scanner saturation." The PSL value (technically, PSL per pixel) can be explicitly computed using equation (5) adapted from J. P. Holder et al.[22]

$$\mathrm{PSL} = S \times 10^{\frac{5}{2}} \frac{4000}{h(V)} \left(\frac{R_{\mathrm{px}}}{100\mu\mathrm{m}}\right)^2 \tag{5}$$

where $h(V)$ is the sensitivity of the PMT, and R_{px} is the pixel size. Here $h(V) = 4000$ and $R_{\mathrm{px}} = 50\mu$m. Note that because the PSL is linearly proportional to the scanner saturation, the ratio of scanner saturation between scans is identical to the ratio of PSL between scans.

IV. ANALYSIS AND RESULTS

The dataset consists of six cases–two IP types at three proton energies–each with five scans. Figure 3 depicts a typical analysis procedure for the trial with an SR image plate with

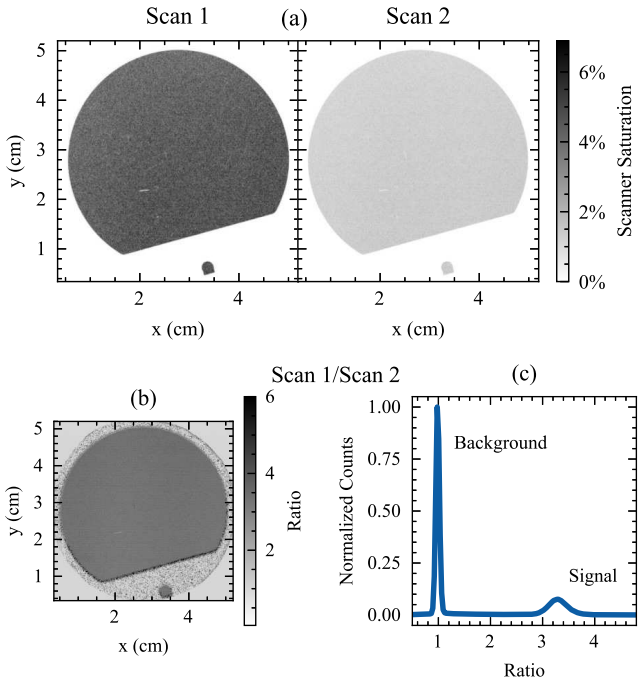

FIG. 3. (a) The first two scans of an SR image plate irradiated with 2.4 MeV protons. The linear scale represents the photo-stimulated luminescence response as a percentage of the peak value the scanner can measure. (b) The spatial distribution for the pixel-by-pixel ratio of scan 1 to scan 2. (c) The histogram of values plotted in figure 3(b).

the 25 μm Al filter. The scanner saturation for each pixel in scan 1 is divided by the scanner saturation for the same pixel in scans 2, 3, 4, and 5 separately. The ratios for all pixels are binned into a histogram. For each ratio histogram, the background region, where ratio ≈ 1, is cut and the statistics of the distribution are computed. The statistics are summarized in box plots for each scan and combination of IP type and post-filter proton energy in Figure 4. The median, the interquartile range, and the 5th and 95th percentiles are plotted.

A number of conclusions can be drawn from Figure 4. As expected, for both IP types and all proton energies, additional scans continue to remove signal. This is evident in the ratio between scan 1 and further scans increasing with scan number. Physically, this is because the scanning laser is not intense enough to remove all trapped electrons with one scan. Signal is removed at a faster rate—a larger ratio over fewer scans—for MS type over SR type IPs. This is expected because the MS type does not contain the blue dye contained in the SR type which attenuates the scanning laser, resulting in less electrons being removed with each scan.

The key result is that the PSL ratio between consecutive scans depends on incident proton energy. For the SR type, there is no intersection between interquartile ranges for any of the incident proton energies. For the MS type the PSL ratio for the 14.0 MeV protons is clearly distinguishable from either the 1.7 MeV or 2.4 MeV protons. The 1.7 MeV and 2.4 MeV protons are not distinguishable from each other. This is likely due to the significant broadening of the PSL ratio distribution for the IP irradiated with 1.7 MeV protons.

In general, broadening of the ratio distribution may occur due to thermal fading, any visible light exposure when handling, or Poisson noise. The case with the widest distribution, the 14.0 MeV protons incident on the SR IP had the lowest

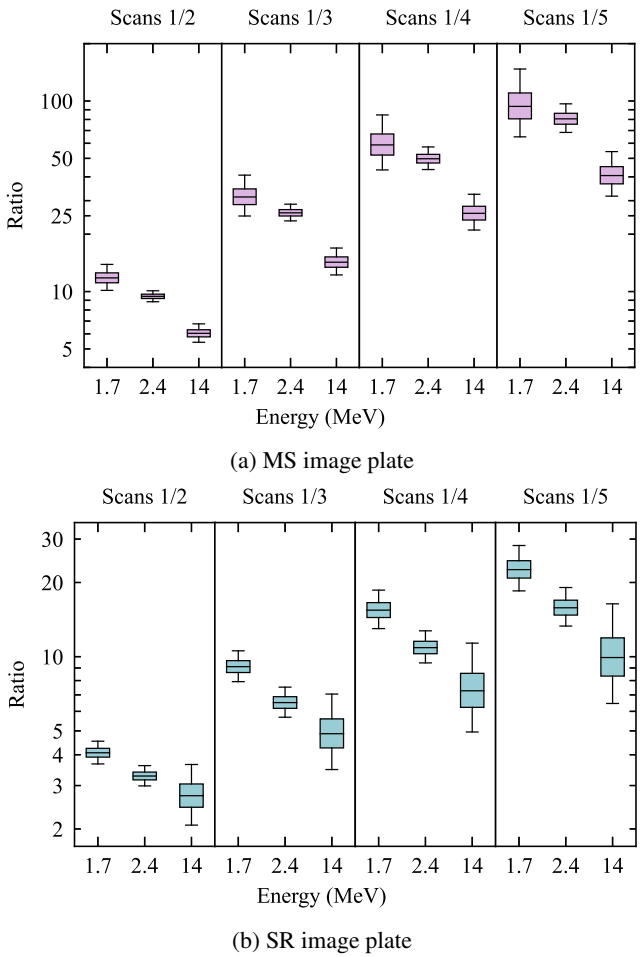

FIG. 4. For MS (a) and SR (b) IPs, the pixel values for scan 1 are divided by the pixel values of scans 2, 3, 4, and 5 to compute the ratios for each proton energy. The distribution of ratio values are represented by box and whisker plots; the filled-in boxes are the interquartile range, the horizontal line is the median, and the whiskers are the 5th and 95th percentiles of the distribution, not error bars.

PSL, at 0.4% of PMT saturation on the first scan. Other trials had between 3% and 20% of PMT saturation on the first scan as shown in Table II. The relative standard deviation, characterizing the width of the PSL signal distribution, is also given in Table II; the standard deviation is highest for this case. It is important to note that while PSL is low in the 5th scans of the 14.0 MeV SR IP and the 1.7 MeV MS IP, the PSL is still well above the background noise of the scanner (66 and 28 times background levels, respectively). This suggests that the extreme broadening in this case is dominated by Poisson noise in the number of trapped electrons removed by the laser.

The physical reason for the PSL ratio depending on proton energy is higher energy protons deposit energy deeper into the IP sensitive layer. This is unrelated to the known differences in absolute sensitivity (PSL/proton) depending on proton energy[11]. Figure 5 plots the proton stopping power dE/dx of the phosphor active layer of both the MS and SR IPs as a function of depth x, for each proton energy E. The stopping power was computed using SRIM stopping power tables[21] with material compositions, thicknesses and densities listed in Table I. The 1.7 MeV and 2.4 MeV protons experience a pronounced Bragg peak in the middle of the sensitive layer, depositing all of their energy, whereas the 14.0 MeV protons

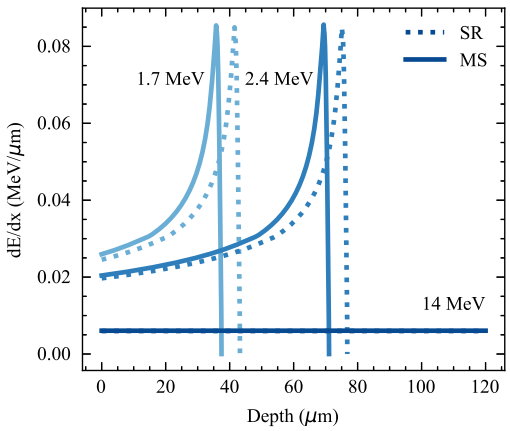

FIG. 5. The stopping power of 1.7, 2.4, and 14.0 MeV protons as a function of depth into the active phosphor layer of MS and SR image plates after having passed through their respective protective layers. The curves are computed using SRIM stopping power tables[21] with material compositions, thicknesses and densities listed in Table I.

pass through depositing minimal energy. When the scanning laser hits the active layer it is attenuated by the phosphor, i.e. the scanning laser is more intense at the front of the sensitive layer and fades in intensity with depth. Trapped electrons are more easily removed at the front of the sensitive layer than in the middle or the back. After the first scan, the trapped electrons at the front have been removed, but deeper trapped electrons remain; the deeper electrons are removed in subsequent scans. Therefore, subsequent scans preferentially probe radiation deposited deeper into the IP. Taking the PSL ratio between subsequent scans reveals differences in the depth of initial energy deposition between protons of different energies. Hence, the PSL ratio between scans differs for IPs irradiated with protons of different energies because the protons deposit energy at different depths in the IP.

V. CONCLUSIONS AND PATH FORWARD

IPs were irradiated with protons of energy ranging from 1.7 MeV to 14.0 MeV and scanned multiple times in succession. Critically, the PSL ratio between subsequent scans was found to depend on proton energy. It was also found that the MS type IP loses signal due to scanning more rapidly than the SR type. High fluence experiments that require scanning the IP many times before the IP is no longer saturated may benefit from using the MS type.

The found energy dependence implies that the scan ratio from subsequent scans of an IP can be used to infer coarse information about the energy of incident protons. This is information that cannot be obtained from one scan alone. The dependence of ratio on proton energy is believed to be due to the energy dependence of the Bragg peak location in the IP sensitive layer. X-rays do not have a Bragg peak, but follow an exponential decay in energy deposition with depth. This suggests that the PSL ratio between scans of an IP irradiated with x-rays would differ from that of protons, except for high energy protons (>10 MeV) and x-rays (>25 keV), in which the two deposition profiles are similar. Indeed, this is found by comparing the results of this paper with those in M. Cufari et al. [14], where the PSL ratio between scans of an IP irradiated with x-rays was found to depend on x-ray energy. This has important implications because IPs are often used in diagnostics, such as proton radiography, that are irradiated with a mixed proton-x-ray fluence.

The results from this paper along with M. Cufari et al. [14] suggest that it may be possible to discriminate between proton and x-ray fluence on an IP in a mixed radiation environment. Using the found energy dependence of PSL ratio, the ratio between scans of an IP irradiated with a characterized mixed proton-x-ray fluence can be used to identify the relative intensities of proton and x-ray signals. Further work will focus on more clearly defining and properly modeling the observed the energy dependence. On future OMEGA experiments using proton radiography, IPs will be scanned multiple times. The PSL ratio between scans will be measured and used to improve the signal to noise ratio in proton data. By comparing the measured PSL ratio to the ratio from the expected proton energies, the relative x-ray fluence can be estimated and corrected for.

ACKNOWLEDGMENTS

This work was supported by the DOE/NNSA CoE under Contract No. DE-NA0003868. This report was prepared as an account of work sponsored by an agency of the United States Government. Neither the United States Government nor any agency thereof, nor any of their employees, makes any warranty, express or implied, or assumes any legal liability or responsibility for the accuracy, completeness, or usefulness of any information, apparatus, product, or process disclosed, or represents that its use would not infringe privately owned rights. Reference herein to any specific commercial product, process, or service by trade name, trademark, manufacturer, or otherwise does not necessarily constitute or imply its endorsement, recommendation, or favoring by the United States Government or any agency thereof. The views and opinions of authors expressed herein do not necessarily state or reflect those of the United States Government or any agency thereof.

DATA AVAILABILITY STATEMENT

The data that support the findings of this study are available from the corresponding author upon reasonable request.

REFERENCES

[1]P. J. Adrian et al., Rev. Sci. Instrum. **93** (2022), 10.1063/5.0101655.
[2]E.R. Tubman et al., Nuc. Instrum. and Methods A **1060**, 169027 (2024).
[3]A. Casner et al., High Power Laser Sci. Eng. **6**, e44 (2018).
[4]T. Ma et al., Rev. Sci. Instrum. **83** (2012), 10.1063/1.4733313.
[5]N. Izumi et al., Rev. Sci. Instrum. **83** (2012), 10.1063/1.4738660.
[6]C. K. Li et al., Phys. Rev. Lett. **97**, 135003 (2006).
[7]A. B. Zylstra et al., Rev. Sci. Instrum. **83**, 013511. (2012), 22299955.
[8]J. R. Rygg et al., Science **319**, 1223 (2008), 18309079.
[9]T. M. Johnson et al., Proc. 25th Top. Conf. HTPD (2024).
[10]G. Sutcliffe et al., Rev. Sci. Instrum. **92** (2021), 10.1063/5.0043845.
[11]A. Mančić et al., Rev. Sci. Instrum. **79** (2008), 10.1063/1.2949388.
[12]P. Martin et al., Rev. Sci. Instrum. **93** (2022), 10.1063/5.0089402.
[13]T. Bonnet et al., Rev. Sci. Instrum. **84**, 013508 (2013).
[14]M. Cufari et al., Proc. 25th Top. Conf. HTPD (2024).
[15]H. Ohuchi et al., Nuc. Instrum. and Methods A **450**, 343 (2000).
[16]B. R. Maddox et al., Rev. Sci. Instrum. **82**, 023111. (2011), 21361577.
[17]Nobuhiko Izumi, private communication (2023).
[18]N. Sinenian et al., Rev. Sci. Instrum. **83**, 043502. (2012), 22559531.
[19]S. Krupakar Murali et al., Fusion Science and Technology **53**, 841 (2008).
[20]N. Izumi et al., SPIE **LLNL-CONF-643255** (2013).
[21]J. F. Ziegler et al., Nuc. Instrum. and Methods B **268**, 1818 (2010).
[22]J. P. Holder et al., Rev. Sci. Instrum. **89** (2018), 10.1063/1.5039363.